Electrochimica Acta 317 (2019) 427–436

Contents lists available at ScienceDirect

Electrochimica Acta

journal homepage: www.elsevier.com/locate/electacta

# Insights into electrodeposition and catalytic activity of $MoS_2$ for hydrogen evolution reaction electrocatalysis

Ramunas Levinas [a, *, 1], Natalia Tsyntsaru [a, b, 1], Henrikas Cesiulis [a]

[a] Faculty of Chemistry and Geosciences, Vilnius University, Naugarduko str. 24, Vilnius, Lithuania
[b] Institute of Applied Physics of ASM, 5 Academiei str., Chisinau, Republic of Moldova

ARTICLE INFO

*Article history:*
Received 13 February 2019
Received in revised form
31 May 2019
Accepted 1 June 2019
Available online 5 June 2019

*Keywords:*
Molybdenum disulfide
Electrodeposition
Active sites
Hydrogen evolution reaction
Electrochemical impedance spectroscopy

ABSTRACT

$MoS_{2-x}$ films were electrodeposited cathodically onto copper rod substrates from a solution, containing $MoS_4^{2-}$ as the common Mo and S ion precursor. The catalyst loading was varied by adjusting electrodeposition conditions – applied potential and deposition time. A typical set of HER electrocatalyst experiments (polarization, Tafel slope analysis) carried out in 0.5 M $H_2SO_4$ was applied on the deposited $MoS_{2-x}$ films. Analysis of surface morphology (SEM) and chemical composition (EDS) were also performed. Electrochemical impedance spectroscopy in the same acidic media was used to evaluate the catalyst-solution interface and the interfacial kinetics (by calculating double layer capacitance and charge transfer resistance), as well as characterize the hydrogen adsorption process (adsorption capacitance and resistance). A linear correlation between electrodeposition time and double layer capacitance was observed. However, the charge transfer resistance was found to decrease until it plateaued at longer deposition times. The $MoS_{2-x}$ film, deposited for 7200 s at −1.0 V (vs. Ag/AgCl), reached 10 mA $cm^{-2}$ HER current at −0.18 V (vs. RHE), and represented the best result of this study. Electrochemical impedance spectroscopy (EIS) was further applied to evaluate the subtle changes in the $MoS_{2-x}$ films' semiconductor properties after HER stability tests (at −40 mA $cm^{-2}$), and to estimate the number of active sites on the material. EIS, in comparison to cyclic voltammetry or roughness factor calculations, is a completely non-destructive method that can be applied to accurately assess the system under investigation.



## 1. Introduction

Contemporary research into renewable energy always faces a common issue, namely: what can be used as an energy carrier from production to consumption. Hydrogen is considered as a potential alternative to hydrocarbons [1], but for a true breakthrough in hydrogen fuel cells more effective methods of $H_2$ generation and storage must be discovered. Photo- or electrochemical water splitting can be a source of clean $H_2$ fuel, but the process is hindered by unfavourable kinetics, and for efficient, large-scale application a catalyst is required [2].

Molybdenum sulphide compounds have been an object of research since at least 1977 [3–5], and have been thoroughly investigated for their semiconductor, photo-, and electrochemical properties. Extensive review papers have also been published recently [6–8].

Their electrocatalytic properties towards the hydrogen evolution reaction were elucidated in an attempt to mimic the effects of biological enzymes [9]. In their seminal work, B. Hinnemann et al. proposed that an ideal catalyst would have a free energy of adsorbed H of $\Delta G^H_0 \approx 0$. In other words, hydrogen evolution catalysis would obey the Sabatier principle: the chemical interactions between the catalyst and the substrate should be "just right"; that is, neither too strong nor too weak. A sufficient understanding of the various active centres is important when working with any heterogeneous catalysis, and this was also the case with molybdenum sulphide. Early research showed, that bulk $MoS_2$ (i.e. the basal plane) is a poor HER catalyst [10]. It became known later that edge sites are one of the active sites for $H_2$ evolution [11], and that HER activity would scale with their amount in the catalyst. However, when comparing edge-site-rich $MoS_2$ flakes with a monolayer film, it was found that the film exhibited much better HER activity, which led to proof of the importance of different active sites – sulphur vacancies ($\Delta G^H_0 \approx -0.095$ eV) [12]. Currently, the active sites of $MoS_2$ are thought to be Mo edge sites

* Corresponding author.
*E-mail address:* ramunas.levinas@chf.vu.lt (R. Levinas).
[1] ISE member.

https://doi.org/10.1016/j.electacta.2019.06.002
0013-4686/

($\Delta G^H_0 \approx 0.115$ eV), S vacancies, and grain boundaries ($\Delta G^H_0 \approx 0.181$–$0.566$ eV). The basal plane is effectively inert at $\Delta G^H_0 \approx 1.218$ eV. It may also be important to mention that not all commercially available $MoS_2$ is equal, as it was found that the HER properties of $MoS_2$, obtained from different suppliers, varies greatly due to different methods of preparation [13].

Coatings of unique compositions, crystallographic structures, surface morphologies, and catalytic properties, have been synthesized using chemical vapour deposition [14,15], hydro- or solvothermal deposition [16–18], the increasingly popular chemical exfoliation method, electrodeposition [19–23], and more. Incorporation of naturally-occurring molybdenite has also been shown to greatly enhance the HER catalytic properties of electrodeposited Ni films in alkaline media [24]. Electrodeposited molybdenum disulphide films consist of nonstoichiometric, amorphous $MoS_{2-x}$ that is particularly active towards HER [25,26]. However, they are less stable in comparison to crystalline $MoS_2$ materials [27]. Some of the earlier studies on the electrodeposition of $MoS_2$ have reported the method involving a cathodic reduction of aqueous ammonium tetrathiomolybdate ($(NH_4)_2MoS_4$) [28]. It was found, that electrodeposition begins at −0.9 V (vs. SCE) and reaches a maximum of 30% current efficiency at −1.2 V to −1.4 V, then decreases at more negative potentials due to hydrogen evolution. A linear correlation was found between the electrodeposited film thickness and the charge passed through the cell. On the other hand, oxidative deposition of tetrathiomolybdate solutions at anodic potentials yields the formation of $MoS_3$ [4,5], which also has attractive electrochemical properties. A mixture of $MoS_2$ and $MoS_3$ has been electrodeposited by applying a potential cycling method between cathodic and anodic deposition modes, resulting in a $MoS_{2+x}$ film possessing mixed electrocatalytic capabilities [29].

The stability of electrodeposited $MoS_2$ seems to be an often-omitted issue. Although most research reports satisfactory or even excellent electrochemical stability, some authors have reported that thicker films (>1 μm) peeled off from the substrate [28,30], and that cracks could appear during drying. Furthermore, for a $MoS_2$ monolayer (grown by CVD and aged for 1 year) XPS analysis showed that the Mo/S ratio decreased from 1 /2 to 1 /1.05 due to oxidation of sulphide sites [31]. Calculations based on Density Functional Theory (DFT) revealed, that on a S-deficient $MoS_2$ surface the kinetic $O_2$ dissociative adsorption barrier is relatively low, meaning that the oxidation (passivation) of active sites is thermodynamically favourable [32]. Edge sites and grain boundaries were also found to be susceptible to oxidation, and it was theorized, that the misfit between the $MoS_2$ and $MoO_3$ lattices may be the cause of the mechanical stress that causes $MoS_2$ cracking [33].

Ultimately, during recent years strides have been made in the understanding of amorphous $MoS_{2-x}$ compounds. Raman spectroscopy experiments have unravelled different S–S bonds in electrodeposited $MoS_2$, representing bridging/shared and terminal disulphide bonds. It was revealed that the structure of $MoS_2$ is a polymer, composed of $[Mo_3S_{13}]^{2-}$ clusters connected via disulphide ligands [34]. This structure is currently thought to explain the empirically observed peculiarities of amorphous $MoS_2$: the unprecedented HER electrocatalytic activity (the active unsaturated $Mo^{IV}$ sites/sulphur vacancies have a favourable $\Delta G^H_0$), the reductive activation of some $MoS_2$ compounds (removal of terminal disulphide ligands, resulting in more unsaturated $Mo^{IV}$ sites), and the cathodic corrosion (shortening of the polymer chains). Taking into account what was mentioned above, the present research is devoted to extending the knowledge into the electrodeposition of $MoS_2$, and its catalytic activity for hydrogen evolution reaction.

## 2. Experimental

***Electrolyte preparation.*** Molybdenum disulphide films were electrodeposited from a solution containing a common precursor of $Mo^{6+}$ and $S^{2-}$ ions – tetrathiomolybdate (TTM/$MoS_4^{2-}$). In order to prepare the electrolyte, ammonium heptamolybdate tetrahydrate ($(NH_4)_6Mo_7O_{24}{}^*4H_2O$) and 60% sodium sulphide hydrate ($Na_2S^*xH_2O$) were mixed in a ratio of $Mo/S = 1/4$. The sulfidation of molybdate ions ($MoO_4^{2-}$) to tetrathiomolybdate is a four-step reaction, where each step is reversible, and the total reaction can be represented as follows:

$$MoO_4^{2-} + 4HS^- + 4H^+ \leftrightarrow MoS_4^{2-} + 4H_2O \quad (1)$$

The pH of the mixture was ~12, and it was acidified up to pH of 7 with sulfuric acid to push the reaction equilibrium towards the product side and to favour the formation of $MoS_4^{2-}$ over the intermediates. The reference indicator of $MoS_4^{2-}$ formation was the solution colour changing to a deep red. 25 ml of 2-propanol was added to the electrolyte in order to decrease surface tension and increase wettability of the working electrode. The final electrolyte composition contained: $C_{MoS_4^{2-}} = 0.025$ M + 10% of 2-propanol. The pH was kept weakly alkaline (pH ~ 8) to prevent precipitation of insoluble $MoS_3$.

***$MoS_2$ electrodeposition.*** All electrochemical measurements were carried out using a standard three-electrode cell set-up (potentiostat/galvanostat Metrohm μAutolab Type III). Unless specified otherwise, all potentials were referenced to Ag/AgCl. The copper rod substrates were prepared to have a 1 $cm^2$ working surface area. They were first polished with a commercial detergent, then immersed in 2 M $H_2SO_4$ to dissolve surface oxides, rinsed with distilled water, and finally degreased with 2-propanol. Initially, linear sweep voltammetry measurements were carried out to determine the electrodeposition potential range in the investigated electrolyte. $MoS_{2-x}$ films were deposited under potentiostatic mode, at various cathodic potentials (−0.8 V to - 1.2 V); or at constant potential (−1.0 V), but for different deposition times (200 s–7200 s). The surface morphology and chemical composition of the electrodeposited $MoS_{2-x}$ films were evaluated using a Hitachi TM 3000 Scanning Electron Microscope with an integrated EDX module.

***Electrocatalytic activity measurements.*** To measure the electrocatalytic activity towards hydrogen evolution, the as-deposited $MoS_2$ films were rinsed with distilled water and immediately transferred to a 0.5 M $H_2SO_4$ solution. A multi-faceted characterization of the obtained $MoS_2$ films towards HER consisted of the following measurements: a) open circuit potential (OCP) determination; b) electrochemical impedance spectroscopy (EIS) at −0.32 V vs. Ag/AgCl (−0.1 V vs. RHE); c) ten linear sweep voltammetry (LSV) curves at 10 mV $s^{-1}$ from OCP to - 40 mA $cm^{-2}$ cut-off condition; d) stability measurement for 20 min at −40 mA $cm^{-2}$.

Registering an electrochemical impedance spectrum before electrocatalytic measurements served two purposes: it allowed analysis of the catalyst in a non-destructive way, and supplied an accurate value of electrolyte resistance (for *iR* correction). Accordingly, all polarization curves were corrected for the *iR* drop.

In addition, EIS was used to estimate the $H^+$ adsorption and double layer capacitances ($C_a$ and $C_{dl}$) of the electrodeposited $MoS_{2-x}$ films. The cathodic overpotential for EIS recording was chosen to be not far from Nernst potential (−0.1 V). HER polarization experiments showed that at this overpotential range the reaction of hydrogen evolution occurs slowly. EIS spectra were measured in the range 10 kHz - 0.1 Hz. An amplitude of 20 mV was used based on the data of performed Kronig-Kramers analysis.

## 3. Results and discussion

### 3.1. Cathodic electrodeposition of $MoS_2$

To develop a necessary understanding of the chosen system, linear sweep voltammetry (LSV) measurements at increasing potential scan rates were performed. The cathodic deposition of $MoS_2$ occurs according to Eq. (2):

$$[MoS_4]^{2-} + 2e^- + 2H_2O \rightarrow MoS_2 + 2HS^- + 2OH^- \quad (2)$$

The open circuit potential was chosen as the starting point and the potential was scanned toward −1.2 V (Fig. 1). At a low scan rate (5 mV $s^{-1}$) no clear reduction peaks can be distinguished. $MoS_{2-x}$ electrodeposition occurs alongside hydrogen evolution. When the potential scan rate is increased to 20 mV $s^{-1}$ and more, a small peak in the reduction region (−1.0 V to −1.15 V) becomes apparent, after which further cathodic current increase results in hydrogen evolution. The peak shift towards more cathodic values with increased potential scan rate suggests slow reaction kinetics, as the current is slow to respond to the swift change in the potential. This may be attributed to a slow charge transfer step or diffusion, but the detailed kinetics of this reaction were not the objective of this study.

Hence, $MoS_{2-x}$ films were deposited under a potentiostatic mode, in the range of −0.8 V to −1.2 V to observe film formation nearby the reduction peak. The surface morphology and chemical composition of as-deposited films depends on the potential applied (Fig. 2). Thin layers that replicate the surface morphology of the substrate are obtained at low cathodic potentials (Fig. 2a). At an intermediate deposition potential of −1.0 V a rough and nodular surface structure with some cracks is formed (Fig. 2b). At even higher potentials (−1.2 V) the deposited films were observed to peel off from the substrate when drying. As was expected from LSV, the increase of the cathodic deposition potential results in higher quantities (in at. %) of Mo and S in the electrodeposits at a constant deposition time (Fig. 2c). Larger quantities of Mo and S can be also obtained by increasing the deposition time (Fig. 2d). Thus, by increasing the deposition time it is possible to carry out electrodeposition at lower potentials, in order to avoid intense hydrogen evolution. As it was mentioned, the as-deposited films are thin, and therefore a strong signal of the Cu substrate is visible in the EDX analysis. However, the atomic % of Cu decreases when a larger amount of Mo and S is deposited at higher potentials or deposition times (Fig. 2c and d). It should be noted, that a significant amount of oxygen is also present in the samples, and its relative amount increases with applied potential. This could be attributed to the following issues: a) some amount of unreacted molybdate from the solution can electrodeposit alongside $MoS_{2-x}$; b) due to the oxidation of $MoS_{2-x}$ active centres in air.

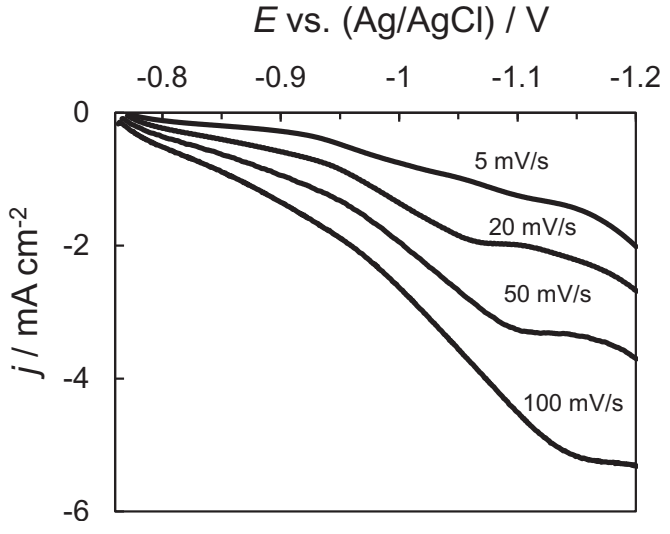


**Fig. 1.** LSV curves of $MoS_{2-x}$ electrodeposition on a bare Cu wire substrate in 25 mM TTM +10% 2-propanol.

### 3.2. Electrocatalytic activity for hydrogen evolution reaction

#### 3.2.1. Influence of electrodeposition potential

The electrodeposited $MoS_{2-x}$ films were all characterized in terms of their ability to catalyse the hydrogen evolution reaction in acidic media. All experiments were carried out with freshly-prepared $MoS_{2-x}$, as it was found that the electrocatalytic activity for HER severely decreases after the films had been dried and stored in air (likely due to surface active site oxidation). Thus, the as-deposited films were removed from the electrolyte, rinsed with distilled water and 2-propanol, and then immediately transferred into 0.5 M $H_2SO_4$. The solution was used for a comprehensive characterization of the obtained films (as described in the experimental section), consisting of EIS, HER voltammetric sweeps, and galvanostatic stability experiments (Fig. 3). Several tendencies were revealed from the analysis.

It is evident that even a thin coating of $MoS_{2-x}$ (deposited at −0.8 V) already greatly increased HER activity compared to the bare substrate (Fig. 3a). An increase in the cathodic deposition potential resulted in better catalytic activity and lower onset overpotentials (measured at 1 mA $cm^{-2}$): 0.232 V and −0.122 V vs. RHE for $MoS_{2-x}$ deposited at −0.8 V and −1.2 V respectively. The reason for this improvement is mostly linked to the increase in catalyst loading, i.e. a higher amount of electrodeposited $MoS_{2-x}$, or a lesser amount of Cu in EDX spectra. A more in-depth analysis of the catalytic activity follows in section 3.3.

The hydrogen evolution rate depends both on the chemical composition of a cathode and surface morphology. An exponential relation between $MoS_{2-x}$ electrodeposition potential and HER exchange current density ($j_0$) was observed (Fig. 3b). Although the average thickness of the films deposited at −1.0 V to −1.2 V does not differ significantly from each other, the increase in $j_0$ is evident. Unfortunately, further increasing of the deposition potential did not obey this exponential relation, probably because of the unfavourable changes in the film's formation that occur due to severe hydrogen evolution.

Another result showing the impact of electrodeposition potential on the intrinsic activity of the film is the calculated HER Tafel slope (Fig. 3c). The mechanism of cathodic hydrogen evolution occurs through a few intermediate stages, and each of these can be rate limiting:

$$Volmer: H^+ + e^- \rightarrow H_{ads} \quad (3)$$

$$Heyrovsky: H_{ads} + H^+ + e^- \rightarrow H_2 \quad (4)$$

$$Tafel: H_{ads} + H_{ads} \rightarrow H_2 \quad (5)$$

If the Volmer adsorption reaction is the rate limiting step, a Tafel slope of 120 mV $dec^{-1}$ would be expected. If either the Heyrovsky or Tafel recombination steps are rate limiting, the Tafel slope would be 40 or 30 mV $dec^{-1}$. For the investigated samples, Tafel slopes generally fell within the 40–50 mV $dec^{-1}$ range, showing mixed HER kinetics. One exception from the given trend was the $MoS_{2-x}$ film, deposited at −1.2 V. The Tafel slope for this sample was markedly higher at 65.9 mV $dec^{-1}$ (Fig. 3c). The increase in the Tafel

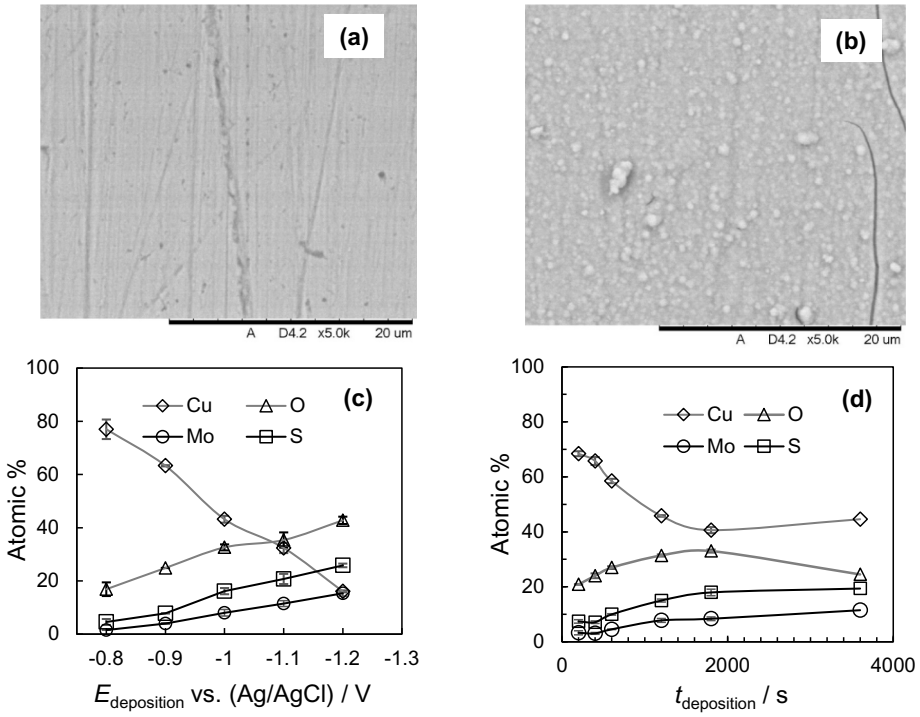


**Fig. 2.** SEM images of the surface morphology of $MoS_{2-x}$ films, electrodeposited for 600 s at −0.8 V and −1.0 V respectively (a, b). Influence of applied potential at fixed deposition time of 600 s (c) and deposition time at fixed potential of −1.0 V (d) on composition of $MoS_{2-x}$ films electrodeposited on copper.

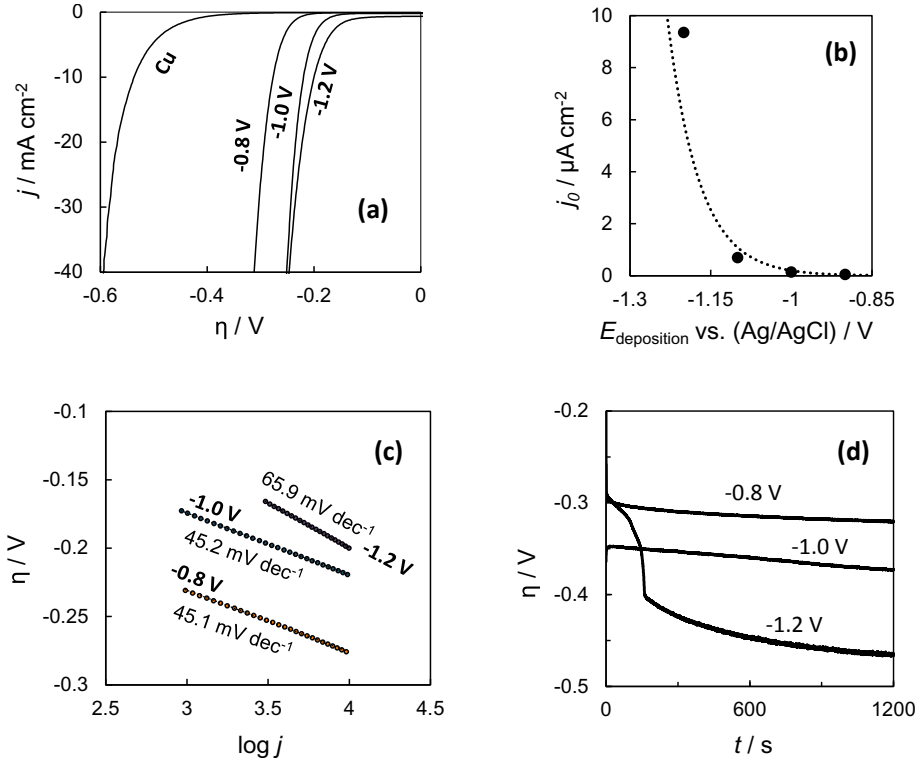


**Fig. 3.** Hydrogen evolution electrocatalysis data: 10th cycle of HER polarization curve of $MoS_{2-x}$ films, electrodeposited at indicated potentials for 600s, scan rate 10 mV $s^{-1}$, 0.5 M $H_2SO_4$. Bare Cu substrate added for comparison (a); HER exchange current density as a function of $MoS_{2-x}$ electrodeposition potential (b); Tafel slopes of the respective samples (c); Galvanostatic (−40 mA $cm^{-2}$) stability experiments (d) – see details in the text.

slope shows an unfavourable deviation from the dominating Volmer-Heyrovsky or Volmer-Tafel HER mechanism. This may be related to the occurrence of side reactions during electrodeposition at this relatively high potential, and the changes in the deposited $MoS_{2-x}$ films. The Mo: S ratio of this film was also the lowest at 1:1.68.

Finally, the electrochemical stability of the $MoS_{2-x}$ films was evaluated by chronopotentiometry at moderately harsh working

conditions of −40 mA cm$^{-2}$ for 20 min (Fig. 3d). On average, the films lost around 5% activity over the measurement, but $MoS_{2-x}$ film deposited at −1.2 V underwent complete destruction (peeling off from the substrate) within the first 200 s of the experiment. These experiments show that, although electrodeposition at higher potentials seems to yield films with better electrocatalytic activity, their stability is unacceptable.

### 3.2.2. Influence of deposition time

Deposition time also affects the elemental composition of the $MoS_{2-x}$ layers (Fig. 2 b), and consequently can change their catalytic activity. Taking into account SEM/EDX analysis and stability of the films, deposition at a constant potential of −1.0 V but for different times (200 s–7200 s) was chosen for further investigation (Fig. 4). Indeed, a longer deposition time had a significant effect on the $MoS_{2-x}$ films' electrocatalytic activity. The overpotential for HER (at 10 mA cm$^{-2}$) changed from −0.285 V to −0.180 V (vs. RHE) when the deposition time was increased from 200 s to 7200 s (Fig. 4a), which may be attributed to increasing catalyst loading. However, a diminishing gain in catalytic activity is observed when deposition times are increased from 1800 s to 7200 s. A limit is reached where the electrode's total catalytic activity no longer depends on catalyst loading.

The exchange current density increases linearly with deposition time in the entire investigated range up to 7200 s (Fig. 4b). This is a particularly promising result, as it implies a possibility to reach relatively high exchange current densities under mild electrodeposition conditions. The Tafel slopes of these samples also show an interesting behaviour (Fig. 4c). A minimum of 42.5 mV dec$^{-1}$ is reached when the $MoS_{2-x}$ film has been deposited for 1800 s. The reason for this outcome could be linked to the formation of different active sites, or that an optimum catalyst loading is reached, where a further increase of deposition time begins to impede charge transfer in the semiconductor $MoS_{2-x}$ material.

The electrochemical stability of these films does not necessarily correlate to their catalytic activity. Stability tests under the previously described conditions showed that thinner (short deposition time) and more compact films can lose less than 1% (in terms of overpotential) of their initial activity over the experiment. For the film deposited for 1800 s, a larger 2.9% decrease in catalytic activity was observed. Finally, the film with the longest deposition time in our experimental series (7200 s) only had a 1.3% loss from initial activity. These results show that the most electrochemically stable $MoS_{2-x}$ films should have either a compact, or a well-evolved and rough surface morphology.

An electrodeposited $MoS_{2-x}$ film with the highest electrocatalytic activity for HER was compared with that of other $MoS_2$ and $WS_2$ based materials, synthesized by various methods (Table 1). It should be pointed out, that due to difficulties in assessing the electrocatalytically active surface area most reported current densities are normalized to a geometric surface area. Usually bigger catalyst loading results in better catalytic activity. In addition, composites with high-surface-area substrates (e.g. carbon cloth, nanowires) have been reported to exhibit the best catalytic activity and stability.

## 3.3. Electrochemical impedance spectroscopy

### 3.3.1. Catalyst-solution interface evaluation

EIS has been shown to provide useful information on HER catalytic materials that is supplementary to more typical experiments like steady-state polarization, and can give insight into the

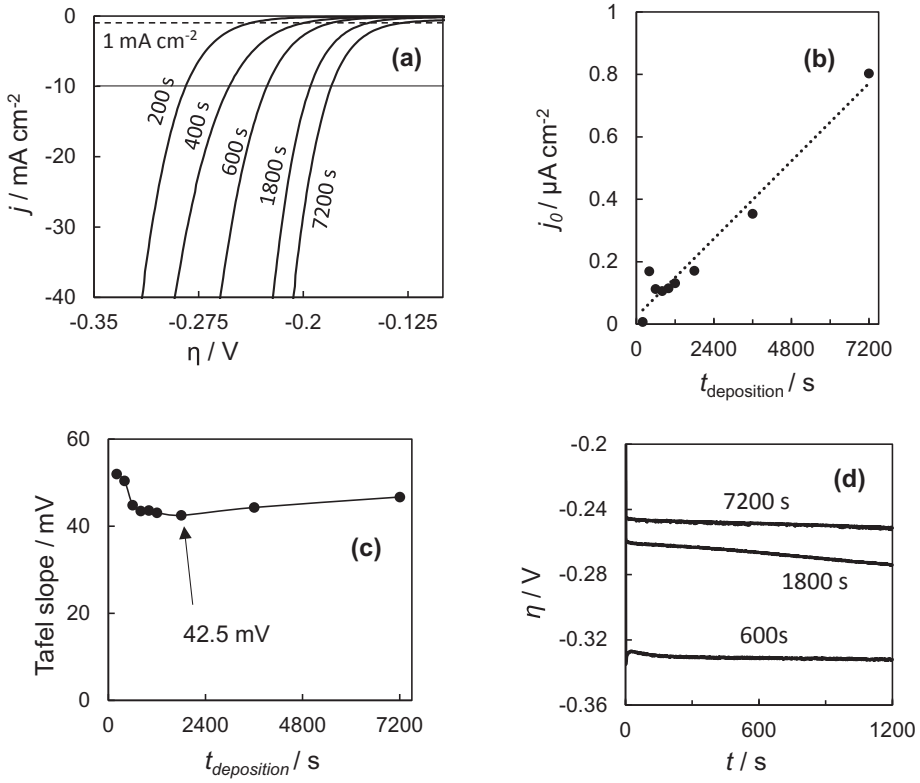


**Fig. 4.** iR-corrected 10th HER polarization curve of $MoS_{2-x}$ films, electrodeposited at −1.0 V (vs. Ag/AgCl) for indicated deposition time (a), scan rate 10 mV s$^{-1}$, 0.5 M $H_2SO_4$; HER exchange current density as a function of deposition time (b); Relation between electrodeposition time and HER tafel slope (c); galvanostatic stability measurement (at −40 mA cm$^{-2}$) curves (d).

**Table 1**
Comparison of key HER catalytic parameters for $WS_2$ and $MoS_2$ based catalysts.

| Catalyst | j/mA cm$^{-2}$ | -E$_j$/mV | Tafel slope/mV dec$^{-1}$ | Synthesis method | Reference |
|---|---|---|---|---|---|
| Ni–$MoS_2$ | 10 | 310 | 47 | Hydrothermal | [35] |
| GO/$WS_2$ | | 180 | 67 | Electrodeposition | [36] |
| VG/CC/$MoS_2$ | | 78 | 53 | Hydrothermal | [37] |
| CC/$CoMoS_x$ | | 100 | 70 | Electrodeposition | [38] |
| GC/$MoS_2$ film | | 202 | 48 | Electrodeposition | [39] |
| CC/$MoS_2$ | 86 | 250 | 50 | Solvothermal | [40] |
| Ti/$MoS_2$ | 30 | 250 | – | Hydrothermal | [41] |
| CC/$WS_2$ | 42 | 300 | 68 | Thermolysis | [42] |
| rGO/$WS_2$ | 23 | 300 | 58 | Hydrothermal | [43] |
| CC/Mo–W–S | 10 | 198 | 54 | Electrodeposition | [44] |
| $MoO_3$–$MoS_2$ | | 254 | – | CVD/sulfidization | [45] |
| Amorph. $MoS_3$ | | 242 | – | Electrodeposition | [25] |
| Exfol. $MoS_2$ | | 207 | – | Liquid exfoliation | [46] |
| $MoS_{2-x}$ | | 180 | 44 | Electrodeposition | This work |

mechanic or kinetic phenomena of the system under investigation [47]. In this study, the EIS spectra were obtained prior to the polarization measurements, in the same working electrolyte of 0.5 M $H_2SO_4$. A cathodic overpotential of −0.1V was chosen, as it represents a potential window where the Faradaic reaction (hydrogen evolution) occurs at a low rate, and a lower disturbance of the pre-electrode layer by hydrogen bubbles is expected.

Under these experimental conditions, the low-frequency current response to the potential perturbation should be caused mainly by the adsorption of H onto the active sites of the $MoS_{2-x}$ film. Because the majority of active centres are S vacancies and Mo edges (with respective free hydrogen adsorption energies of $\Delta G^H{}_0 \approx -0.095$ eV, $\Delta G^H{}_0 \approx 0.115$ eV [12]), specific $H^+$ adsorption had to assert during measurements by EIS and further characterization of the catalyst-solution interface. The characteristic impedance spectra are shown in Fig. 5. An identical high-frequency inductive response was observed for all samples. Although it did not seem to vary with electrodeposition time (and as such was likely not related to the occurring changes in the electrodeposited $MoS_{2-x}$ films), it was also taken into account when fitting the data to equivalent electrochemical circuit models.

All of the impedance spectra have an almost entirely capacitive profile in the low-frequency range, but at higher frequencies (~1000 Hz–100 Hz) the beginning of a small semicircle can be distinguished (see Fig. 5a and insert). As is seen from Bode plots (Fig. 5b and c), a longer deposition time resulted in lower impedance magnitudes. When a thicker layer of a semiconductor is deposited, an opposite result would be expected – the impedance magnitude should increase. It confirms that the measured EIS spectra reflect the electrocatalytic activity of the $MoS_{2-x}$ films. However, in order to model the spectra using discrete elements, both the double layer and adsorption capacitances should be taken into account. Therefore, the equivalent electric circuit (EEC) used for fitting has to involve elements attributed to the capacitance of the double electric layer ($C_{dl}$) and capacitance describing the specific adsorption of hydrogen onto the active sites of $MoS_{2-x}$ film ($C_a$). Thus, the results were fitted to the EEC shown in Fig. 6.

This EEC has been often used to model reactions with a consecutive adsorption step. The inductance element has been added in order to fit the spectrum in the entire measured frequency range. The quality of the fit was evaluated by the chi-square and lowest sum of squares tests, by checking the randomness of the fit residuals, low relative standard deviations (normally less than 5%), and applying statistical F-test and *t*-test analysis. The model was found to fit the spectra well and conforms the requirements of performed statistical tests.

A constant phase element ($CPE_a$, Fig. 6) fits the experimental data better than a simple capacitance element; the obtained values of $T$ were recalculated into capacitance, $C_a$, using Brug et al.'s formula, Eq. (6) [48]:

$$C_a = T_a^{\frac{1}{n}}\left(\frac{1}{R_s + R_{ct}} + \frac{1}{R_a}\right)^{1-\frac{1}{n}} \quad (6)$$

where $T_a$ is the parameter related to the electrode capacitance, $n$ is the constant phase exponent; $R_s$, $R_{ct}$ and $R_a$ are uncompensated, charge transfer, and adsorption resistances, respectively.

This EEC describes an EIS spectrum that has two time constants. The process occurring at high frequencies is characterized by ($C_{dl}$–$R_{ct}$), and the corresponding time constant is $\tau_1$. Here $C_{dl}$ is the double-layer capacitance, and $R_{ct}$ is the charge transfer resistance of the Faradaic process. The ($CPE_a$-$R_a$) circuit represents the low frequency time constant $\tau_2$. Its presence is caused by the hydrogen adsorption reaction. Some variation becomes evident when the time constants are plotted against the electrodeposition time of the $MoS_{2-x}$ films (Fig. 7). The high frequency time constant $\tau_1$ approaches a maximum of 0.067 s, and the low frequency $\tau_2$ reaches a minimum of 1.48 s for the film electrodeposited for 1000 s, and is lowest for films that have been deposited for 400–1200 s. This tendency broadly corresponds to the change in Tafel slope. As it is seen in Fig. 4d, although the total electrode activity increases with deposition time, part of that increase should be attributed to changes in the electrocatalytically active surface area rather than the intrinsic activity of the material.

The variations of the double layer capacitance $C_{dl}$, adsorption capacitance $C_a$, and adsorption resistance $R_a$ are presented in Fig. 8. Both $C_{dl}$ and $C_a$ increase with deposition time, but the double layer capacitance at shorter deposition times remains larger than $C_a$. Such high values of $C_{dl}$ are defined by a large real area of the obtained surface in comparison with the flat geometric surface area. Therefore, it is even higher than $C_a$, whose values are defined by both the roughness of the surface and electric current response to the reversible variations of surface coverage of adsorbate under the electrode potential perturbation during faradaic hydrogen evolution process.

However, when the films have been deposited for 1800 s and longer, the adsorption capacitance grows larger than $C_{dl}$. This is likely related to an increase in the number of active sites, and a consequent increase of coverage of the electrode surface by $H_{ads}$. The adsorption-related resistance $R_a$ follows an exponential extinction curve, and almost plateaus at 226 Ω cm$^2$ for the longest deposition time film, which could be attributed to the appearance of charge transfer limitations in the growing $MoS_{2-x}$ film.

This can be further related to the observed limit in HER

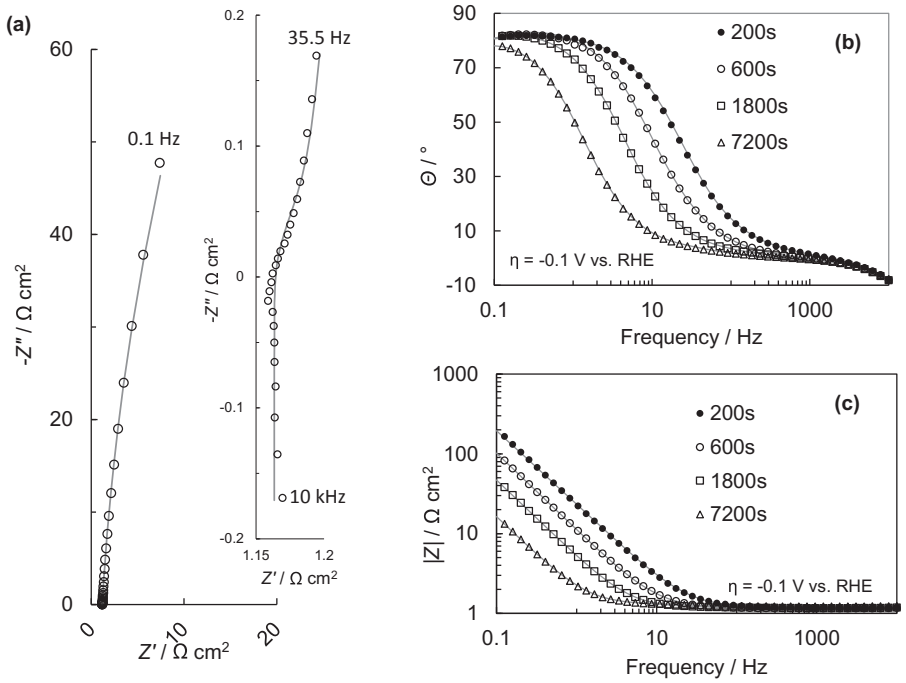


**Fig. 5.** EIS spectra obtained at overpotential −0.1 V of $MoS_{2-x}$ films, electrodeposited for different deposition times: a representative complex-plane Nyquist spectrum of a $MoS_{2-x}$ film electrodeposited for 1800 s (inset shows high frequency region) (a); the Bode impedance plots for respective films (b, c). Lines represent fitted data.

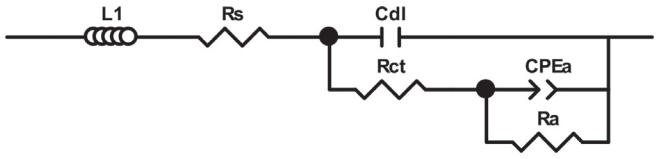


**Fig. 6.** Equivalent electric circuit used for EIS data fitting. $L_1$ – inductance element. $R_s$ – electrolyte resistance; $C_{dl}$ – element representing double layer capacitance; $R_{ct}$ – Faradaic charge transfer resistance; $CPE_a$ – constant phase element of the adsorption reaction; $R_a$ – adsorption resistance.

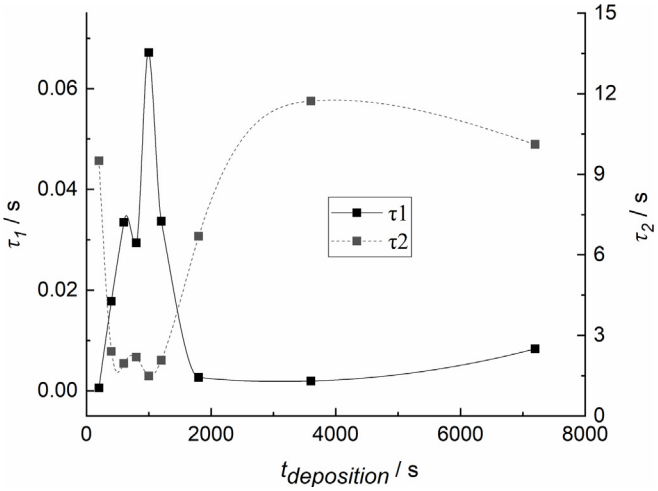


**Fig. 7.** The variation of time constants $\tau_1$ (high frequency) and $\tau_2$ (low frequency) with electrodeposition time.

electrocatalytic activity for the investigated films. With increasing film deposition time, the $\eta_{10mA}$ (overpotential at 10 mA cm$^{-2}$ of HER current) and HER onset overpotential reach a plateau (Fig. 9). Thus, although further catalyst loading by electrodeposition is possible, the gain in electrocatalytic activity remains almost constant. In order to construct a more active electrode for HER electrocatalysis, it would be best to choose an optimal deposition time that results in better intrinsic activity, and increase the surface area of the substrate.

### 3.3.2. Electrochemical stability

The EIS methodology has also been applied to characterize the film and the catalyst-solution interface before and after stability tests (20 min under galvanostatic conditions at −40 mA cm$^{-2}$). A first EIS spectrum was generated prior to the test, and the second after, in the same electrolyte and applied conditions. The procedure allowed tracking any changes in the surface morphology, structure, or composition of the catalyst, by evaluating the differences in the impedance spectra. Indeed, a small but detectable signal was observed. Namely, the impedance magnitudes $|Z|$ and phase angles $\theta$ increased slightly after stability tests. The changes of the double layer and adsorption capacitances, as well as the charge transfer resistance, were estimated using the same EEC shown in Fig. 6. $C_{dl}$ was found to decrease slightly after the stability test, which likely shows a decrease of the electrochemically active surface area. However, the $R_a$ increased up to several hundred ohms for some samples. This correlates with the cathodic corrosion of amorphous $MoS_{2-x}$ in the form of shortening $[Mo_3S_{13}]^{2-}$ polymer chains that has been hypothesized in Ref. [34]. A disrupted polymeric structure would indeed result in a hindered charge transfer step. These EIS results correspond well with the voltammetric stability curves (Fig. 4d). The capacitance of the specifically adsorbed species also changes after stability tests, and $C_a$ was seen to increase slightly. The increase in adsorption capacitance is likely caused by another phenomenon related to the polymeric structure – the removal of terminal disulphide ligands, which results in the appearance of

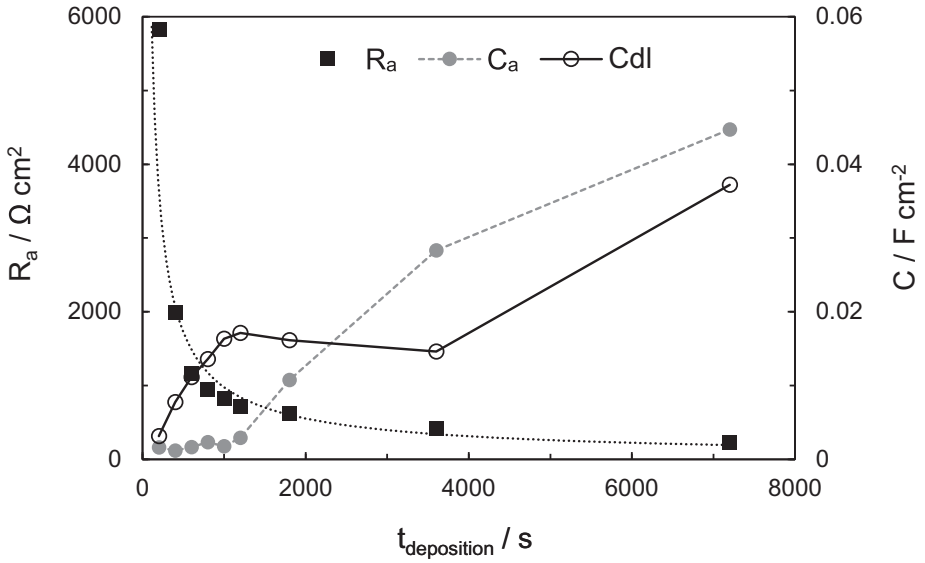


**Fig. 8.** EEC-calculated values of $C_{dl}$, $C_a$ and $R_a$, and their dependence on the electrodeposition time of $MoS_{2-x}$ films.

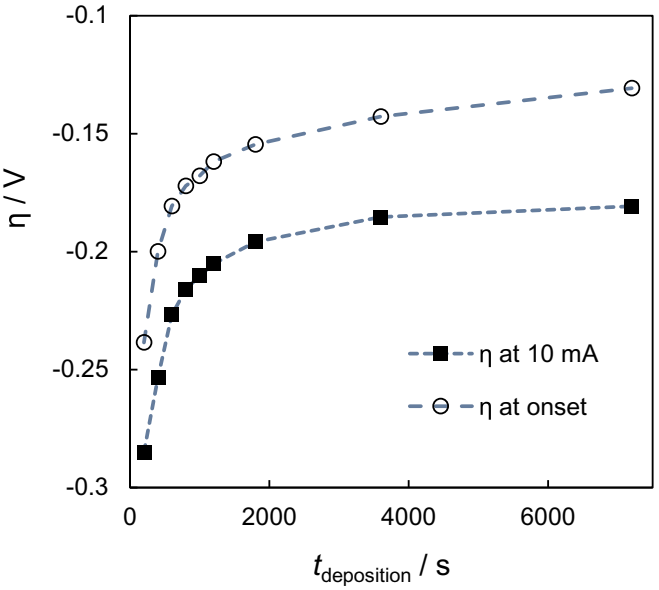


**Fig. 9.** HER onset overpotential (at $-1\ mA\ cm^{-2}$) and overpotential, needed to reach $10\ mA\ cm^{-2}$ of HER current, as a function of electrodeposition time.

new active sites (unsaturated $Mo^{IV}$ sites). These experiments prove that, under vigorous hydrogen evolution conditions, the $MoS_{2-x}$ films actually gain some active sites, but lose electrocatalytically active surface area and charge transfer conductivity, which limits the overall HER electrocatalytic activity of the material.

### 3.3.3. Estimation of electrocatalytically active sites

The electrocatalytically active surface area is not necessarily equal to the electrochemically active surface area, and attempts to normalize HER current density into electrochemically active surface area can skew the desired results. It should be noted, that there is no conventional method for active site calculation yet; research on $MoS_2$-based HER catalysts usually faces difficulty in finding an appropriate way for number of active site estimation. However, researchers often report the number of active sites per $cm^2$ to compare their synthesized materials. Therefore, a following model to estimate the number of active sites attributed to the specific adsorption of $H_{ads}$ by the application of EIS is discussed.

Firstly, to have a baseline for comparison, a calculation for a theoretical ideal catalytic film with 100% adsorbed hydrogen coverage is performed. From a geometrical point of view, an active site (sulphur vacancy) on the surface of a $MoS_{2-x}$ lattice has a diameter of ~0.5 nm [12]. Therefore, a film of 1 $cm^2$ would then have $5.0 \cdot 10^{14}$ active sites. Assuming complete coverage with a monolayer of $H_{ads}$, the charge necessary to attain this monolayer would be $\sigma = 0.08$ mC.

For the $MoS_2$ films, the charge necessary to attain a layer of adsorbed H was calculated from the EIS data, by taking into account only the adsorption capacitance. Values of $C_a$ were recalculated into charge using following equation:

$$Q_a = C_a \eta \tag{7}$$

where $Q_a$ is the charge used to obtain a layer of $H_{ads}$ on the $MoS_{2-x}$ film's surface; $C_a$ is the adsorption capacitance; η is the overpotential applied for hydrogen evolution reaction, and at the same time for $H_{ads}$ layer formation (−0.1 V).

It was assumed, that hydrogen adsorption is a one-electron process (Eq. (3)), and the one active site adsorbs a single $H^+$. Thus, the maximum number of active sites can be calculated from Equation (8).

$$N_{sites} = \frac{Q_a * N_A}{nF} \tag{8}$$

This yields values ranging from $10^{15}$ to $10^{16}$ sites $cm^{-2}$ (see Table 2). Taking into account the difference between the real surface area and the geometric, these values are considered as being in good agreement with those obtained from geometric parameters as described above. In addition, the values estimated based on $C_a$ data are close to those reported by other researchers working with different methods (e.g. roughness factor/capacitance calculations,

**Table 2**
Adsorption charge and active site calculation data.

| $t_{deposition}$/s | $Q_a$/mC $cm^{-2}$ | $N_{active\ sites} \cdot 10^{15}$/sites $cm^{-2}$ |
|---|---|---|
| 200 | 0.22 | 1.02 |
| 600 | 0.183 | 1.05 |
| 1200 | 0.317 | 1.81 |
| 3600 | 3.19 | 17.7 |
| 7200 | 5.05 | 27.9 |

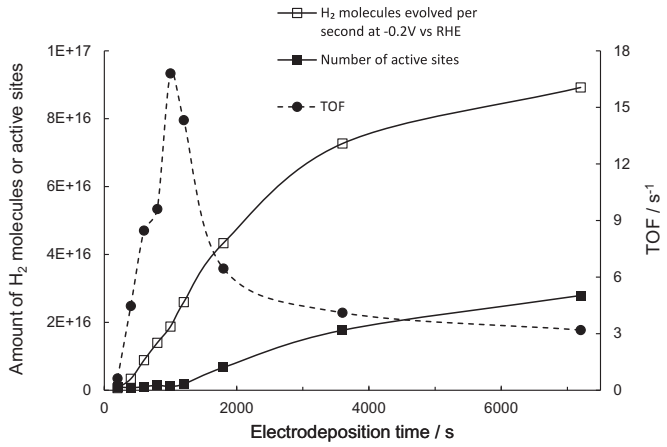


**Fig. 10.** Number of active sites and HER turnover frequencies at −0.2 V vs. RHE of $MoS_{2-x}$ films, electrodeposited for different times (200 s–7200 s).

anodic oxidation, etc) to estimate active site densities for amorphous $MoS_{2-x}$ [25,49].

The turnover frequencies (number of hydrogen molecules evolved per active site per second) for the films were compared at an overpotential of −0.2 V (Fig. 10). Active site number values per 1 $cm^2$ of the geometric area of the deposits were calculated from EIS data as described previously. The number of $H_2$ molecules evolved per second was calculated from respective current densities at overpotential −0.2 V, assuming that hydrogen evolution is a two-electron process. A maximum of turnover frequencies (TOF) of 15.3 $s^{-1}$ was calculated for the $MoS_{2-x}$ film, electrodeposited for 1000 s. Although the films, deposited for longer times (up to 7200 s) have better total activity, probably because of an optimum point in deposition time for per-site activity. These data also correspond well to the results presented in Fig. 4c, where the films deposited for 400 s–1800 s had the lowest Tafel slopes ranging from 42 to 44 mV $dec^{-1}$. A Tafel slope close to 40 mV $dec^{-1}$ suggests that hydrogen evolution occurs through a Volmer-Heyrovsky mechanism, and that the electrochemical desorption (Heyrovsky) step is rate limiting [50,51]. The calculated turnover frequencies are in agreement with these data: the highest TOFs correspond to the lowest Tafel slopes. In addition, comparing the results with the time constants presented in Fig. 7, the same correlation is seen: the lowest adsorption time constants correspond to the highest turnover frequencies. The agreement between polarization and electrochemical impedance experiments again confirms the validity of using EIS to approximate the number of active sites on electrodeposited $MoS_{2-x}$.

Electrochemical impedance spectroscopy can be proposed as a simple way to determine various HER electrocatalyst properties: from activity and stability to the number of active sites and/or turnover frequency. Under carefully chosen electrochemical conditions, it is an entirely non-destructive method that can be seamlessly included in the experimental procedure and provide valuable data on the film/solution interface.

## 4. Conclusions

Nonstoichiometric $MoS_{2-x}$ films were electrodeposited on copper substrates from a $MoS_4^{2-}$ ion solution under potentiostatic conditions (−0.8 V to −1.2 V). It was found that electrodeposition at −1.0 V vs. Ag/AgCl provided more stable films, and this potential was taken as a reference to study the influence of the deposition time (200 s–7200 s) on the electrocatalytic activity of as-deposited films. A $MoS_{2-x}$ film, deposited for 7200 s, was comparable in terms of HER electrocatalytic activity to some of the best reported in the field so far (−0.18 V vs. RHE at 10 mA $cm^{-2}$). However, charge transfer limitations within the semiconductor lattice were found to limit catalytic activity. Under galvanostatic stability testing conditions (−40 mA $cm^{-2}$) the film lost ~1,3% of its initial activity over a period of 20 min. The loss in activity has been hypothesized to be caused by a shortening of polymeric $[Mo_3S_{13}]^{2-}$ chains. Electrochemical impedance spectroscopy measurements confirmed this, showing an increase in charge transfer resistance after the stability tests. EIS was also applied to estimate the active site density on the electrodeposited $MoS_{2-x}$. Values in the range of $10^{15} \div 10^{16}$ active sites $cm^{-2}$ were obtained. The number of active sites increased with deposition time, and followed the same trend as the exchange current density.

## Acknowledgements

Authors acknowledge funding from H2020 project SMARTELECTRODES (No.778357) and by Research Council of Lithuania No 09.3.3-LMT-K-712-08-0003.

## References

[1] M.S. Dresselhaus, I.L. Thomas, Alternative energy technologies, Nature 414 (2001) 332–337, https://doi.org/10.1038/35104599.
[2] M.G. Walter, E.L. Warren, J.R. McKone, S.W. Boettcher, Q. Mi, E.A. Santori, N.S. Lewis, Solar water splitting cells, Chem. Rev. 110 (2010) 6446–6473, https://doi.org/10.1021/cr1002326.
[3] H. Tributsch, J.C. Bennett, Electrochemistry and photochemistry of $MoS_2$ layer crystals. I, J. Electroanal. Chem. 81 (1977) 97–111, https://doi.org/10.1016/S0022-0728(77)80363-X.
[4] R.N. Bhattacharya, C.Y. Lee, F.H. Pollak, D.M. Schleich, Optical study of amorphous $MoS_3$: determination of the fundamental energy gap, J. Non-Cryst. Solids 91 (1987) 235–242, https://doi.org/10.1016/S0022-3093(87)80306-X.
[5] G. Laperriere, B. Marsan, D. Belanger, Preparation and characterization of electrodeposited amorphous molybdenum sulfide, Synth. Met. 29 (1989) 201–206, https://doi.org/10.1016/0379-6779(89)90900-4.
[6] A.S. Aliyev, M. Elrouby, S.F. Cafarova, Electrochemical synthesis of molybdenum sulfide semiconductor, Mater. Sci. Semicond. Process. 32 (2015) 31–39, https://doi.org/10.1016/j.mssp.2015.01.006.
[7] Z. He, W. Que, Molybdenum disulfide nanomaterials: structures, properties, synthesis and recent progress on hydrogen evolution reaction, Appl. Mater. Today. 3 (2016) 23–56, https://doi.org/10.1016/j.apmt.2016.02.001.
[8] J. Theerthagiri, R.A. Senthil, B. Senthilkumar, A. Reddy Polu, J. Madhavan, M. Ashokkumar, Recent advances in $MoS_2$ nanostructured materials for energy and environmental applications – a review, J. Solid State Chem. 252 (2017) 43–71, https://doi.org/10.1016/j.jssc.2017.04.041.
[9] B. Hinnemann, P.G. Moses, J. Bonde, K.P. Jørgensen, J.H. Nielsen, S. Horch, I. Chorkendorff, J.K. Nørskov, Biomimetic hydrogen evolution: $MoS_2$ nanoparticles as catalyst for hydrogen evolution, J. Am. Chem. Soc. 127 (2005) 5308–5309, https://doi.org/10.1021/ja0504690.
[10] W. Jaegermann, H. Tributsch, Interfacial properties of semiconducting transition metal chalcogenides, Prog. Surf. Sci. 29 (1988) 1–167, https://doi.org/10.1016/0079-6816(88)90015-9.
[11] T.F. Jaramillo, K.P. Jørgensen, J. Bonde, J.H. Nielsen, S. Horch, I. Chorkendorff, Identification of active edge sites for electrochemical $H_2$ evolution from $MoS_2$ nanocatalysts, Science 317 (2007) 100–102, https://doi.org/10.1126/science.1141483.
[12] G. Li, D. Zhang, Q. Qiao, Y. Yu, D. Peterson, A. Zafar, R. Kumar, S. Curtarolo, F. Hunte, S. Shannon, Y. Zhu, W. Yang, L. Cao, All the catalytic active sites of $MoS_2$ for hydrogen evolution, J. Am. Chem. Soc. 138 (2016) 16632–16638, https://doi.org/10.1021/jacs.6b05940.
[13] X.J. Chua, S.M. Tan, X. Chia, Z. Sofer, J. Luxa, M. Pumera, The origin of $MoS_2$ significantly influences its performance for the hydrogen evolution reaction due to differences in phase purity, Chem. Eur J. 23 (2017) 3169–3177, https://doi.org/10.1002/chem.201605343.
[14] X. Wang, H. Feng, Y. Wu, L. Jiao, Controlled synthesis of highly crystalline $MoS_2$ flakes by chemical vapor deposition, J. Am. Chem. Soc. 135 (2013) 5304–5307, https://doi.org/10.1021/ja4013485.
[15] Y. Zhan, Z. Liu, S. Najmaei, P.M. Ajayan, J. Lou, Large-area vapor-phase growth and characterization of $MoS_2$ atomic layers on a $SiO_2$ substrate, Small 8 (2012) 966–971, https://doi.org/10.1002/smll.201102654.
[16] X. Zeng, W. Qin, Synthesis of $MoS_2$ nanoparticles using $MoO_3$ nanobelts as precursor via a PVP-assisted hydrothermal method, Mater. Lett. 182 (2016) 347–350, https://doi.org/10.1016/j.matlet.2016.07.026.
[17] T. Wang, J. Li, G. Zhao, Synthesis of $MoS_2$ and $MoO_3$ hierarchical

nanostructures using a single-source molecular precursor, Powder Technol. 253 (2014) 347–351, https://doi.org/10.1016/j.powtec.2013.12.005.
[18] F. Ye, H. Li, H. Yu, S. Chen, X. Quan, Hydrothermal fabrication of few-layer $MoS_2$ nanosheets within nanopores on $TiO_2$ derived from MIL-125(Ti) for efficient photocatalytic $H_2$ evolution, Appl. Surf. Sci. 426 (2017) 177–184, https://doi.org/10.1016/j.apsusc.2017.07.087.
[19] L.C. Wang, S.K. Bao, J. Luo, Y.H. Wang, Y.C. Nie, J.P. Zou, Efficient exfoliation of bulk $MoS_2$ to nanosheets by mixed-solvent refluxing method, Int. J. Hydrogen Energy 41 (2016) 10737–10743, https://doi.org/10.1016/j.ijhydene.2016.03.206.
[20] X. Chia, A.Y.S. Eng, A. Ambrosi, S.M. Tan, M. Pumera, Electrochemistry of nanostructured layered transition-metal dichalcogenides, Chem. Rev. 115 (2015) 11941–11966, https://doi.org/10.1021/acs.chemrev.5b00287.
[21] H. Lin, J. Wang, Q. Luo, H. Peng, C. Luo, R. Qi, R. Huang, J. Travas-Sejdic, C.G. Duan, Rapid and highly efficient chemical exfoliation of layered $MoS_2$ and $WS_2$, J. Alloy. Comp. 699 (2017) 222–229, https://doi.org/10.1016/j.jallcom.2016.12.388.
[22] H. Ma, Z. Shen, S. Ben, Understanding the exfoliation and dispersion of $MoS_2$ nanosheets in pure water, J. Colloid Interface Sci. 517 (2018) 204–212, https://doi.org/10.1016/j.jcis.2017.11.013.
[23] H. Liu, L. Xu, W. Liu, B. Zhou, Y. Zhu, L. Zhu, X. Jiang, Production of mono- to few-layer $MoS_2$ nanosheets in isopropanol by a salt-assisted direct liquid-phase exfoliation method, J. Colloid Interface Sci. 515 (2018) 27–31, https://doi.org/10.1016/j.jcis.2018.01.023.
[24] L.B. Albertini, A.C.D. Angelo, E.R. Gonzalez, A nickel molybdenite cathode for the hydrogen evolution reaction in alkaline media, J. Appl. Electrochem. 22 (1992) 888–892, https://doi.org/10.1007/BF01023735.
[25] D. Merki, S. Fierro, H. Vrubel, X. Hu, Amorphous molybdenum sulfide films as catalysts for electrochemical hydrogen production in water, Chem. Sci. 2 (2011) 1262–1267, https://doi.org/10.1039/c1sc00117e.
[26] D. Merki, H. Vrubel, L. Rovelli, S. Fierro, X. Hu, Fe, Co, and Ni ions promote the catalytic activity of amorphous molybdenum sulfide films for hydrogen evolution, Chem. Sci. 3 (2012) 2515–2525, https://doi.org/10.1039/c2sc20539d.
[27] J.D. Benck, T.R. Hellstern, J. Kibsgaard, P. Chakthranont, T.F. Jaramillo, Catalyzing the hydrogen evolution reaction ( HER ) with molybdenum sulfide nanomaterials, ACS Catal. 4 (2014) 3957–3971.
[28] E.A. Ponomarev, M. Neumann-Spallart, G. Hodes, C. Lévy-Clément, Electrochemical deposition of $MoS_2$ thin films by reduction of tetrathiomolybdate, Thin Solid Films 280 (1996) 86–89, https://doi.org/10.1016/0040-6090(95)08204-2.
[29] H. Vrubel, X. Hu, Growth and activation of an amorphous molybdenum sulfide hydrogen evolving catalyst, ACS Catal. 3 (2013) 2002–2011, https://doi.org/10.1021/cs400441u.
[30] S.K. Ghosh, T. Bera, O. Karacasu, A. Swarnakar, J.G. Buijnsters, J.P. Celis, Nanostructured MoSx-based thin films obtained by electrochemical reduction, Electrochim. Acta 56 (2011) 2433–2442, https://doi.org/10.1016/j.electacta.2010.10.065.
[31] J. Gao, B. Li, J. Tan, P. Chow, T.M. Lu, N. Koratkar, Aging of transition metal dichalcogenide monolayers, ACS Nano 10 (2016) 2628–2635, https://doi.org/10.1021/acsnano.5b07677.
[32] S. KC, R.C. Longo, R.M. Wallace, K. Cho, Surface oxidation energetics and kinetics on $MoS_2$ monolayer, J. Appl. Phys. 117 (2015) 135301, https://doi.org/10.1063/1.4916536.
[33] J. Martincová, M. Otyepka, P. Lazar, Is single layer $MoS_2$ stable in the air? Chem. Eur J. (2017) 13233–13239, https://doi.org/10.1002/chem.201702860.
[34] P.D. Tran, T.V. Tran, M. Orio, S. Torelli, Q.D. Truong, K. Nayuki, Y. Sasaki, S.Y. Chiam, R. Yi, I. Honma, J. Barber, V. Artero, Coordination polymer structure and revisited hydrogen evolution catalytic mechanism for amorphous molybdenum sulfide, Nat. Mater. 15 (2016) 640–646, https://doi.org/10.1038/nmat4588.
[35] D. Wang, X. Zhang, Y. Shen, Z. Wu, Ni-doped $MoS_2$ nanoparticles as highly active hydrogen evolution electrocatalysts, RSC Adv. 6 (2016) 16656–16661, https://doi.org/10.1039/C6RA02610A.
[36] Z. Pu, Q. Liu, A.M. Asiri, A.Y. Obaid, X. Sun, One-step electrodeposition fabrication of graphene film-confined $WS_2$ nanoparticles with enhanced electrochemical catalytic activity for hydrogen evolution, Electrochim. Acta 134 (2014) 8–12, https://doi.org/10.1016/j.electacta.2014.04.092.
[37] Z. Zhang, W. Li, M.F. Yuen, T.W. Ng, Y. Tang, C.S. Lee, X. Chen, W. Zhang, Hierarchical composite structure of few-layers $MoS_2$ nanosheets supported by vertical graphene on carbon cloth for high-performance hydrogen evolution reaction, Nano Energy 18 (2015) 196–204, https://doi.org/10.1016/j.nanoen.2015.10.014.
[38] N. Zhang, W. Ma, F. Jia, T. Wu, D. Han, L. Niu, Controlled electrodeposition of $CoMoS_x$ on carbon cloth: a 3D cathode for highly-efficient electrocatalytic hydrogen evolution, Int. J. Hydrogen Energy 41 (2016) 3811–3819, https://doi.org/10.1016/j.ijhydene.2015.12.173.
[39] A. Ambrosi, M. Pumera, Templated electrochemical fabrication of hollow molybdenum sulfide microstructures and nanostructures with catalytic properties for hydrogen production, ACS Catal. 6 (2016) 3985–3993, https://doi.org/10.1021/acscatal.6b00910.
[40] Y. Yan, B. Xia, N. Li, Z. Xu, A. Fisher, X. Wang, Vertically oriented $MoS_2$ and $WS_2$ nanosheets directly grown on carbon cloth as efficient and stable 3-dimensional hydrogen-evolving cathodes, J. Mater. Chem. A. 3 (2015) 131–135, https://doi.org/10.1039/C4TA04858J.
[41] Z. Lu, W. Zhu, X. Yu, H. Zhang, Y. Li, X. Sun, X. Wang, H. Wang, J. Wang, J. Luo, X. Lei, L. Jiang, Ultrahigh hydrogen evolution performance of under-water "superaerophobic" $MoS_2$ nanostructured electrodes, Adv. Mater. 26 (2014) 2683–2687, https://doi.org/10.1002/adma.201304759.
[42] T.Y. Chen, Y.H. Chang, C.L. Hsu, K.H. Wei, C.Y. Chiang, L.J. Li, Comparative study on $MoS_2$ and $WS_2$ for electrocatalytic water splitting, Int. J. Hydrogen Energy 38 (2013) 12302–12309, https://doi.org/10.1016/j.ijhydene.2013.07.021.
[43] J. Yang, D. Voiry, S.J. Ahn, D. Kang, A.Y. Kim, M. Chhowalla, H.S. Shin, Two-dimensional hybrid nanosheets of tungsten disulfide and reduced graphene oxide as catalysts for enhanced hydrogen evolution, Angew. Chem. Int. Ed. 52 (2013) 13751–13754, https://doi.org/10.1002/anie.201307475.
[44] C. Li, X. Bo, M. Li, L. Guo, Facile electrodeposition fabrication of molybdenum-tungsten sulfide on carbon cloth for electrocatalytic hydrogen evolution, Int. J. Hydrogen Energy 42 (2017) 15479–15488, https://doi.org/10.1016/j.ijhydene.2017.05.046.
[45] Z. Chen, D. Cummins, B.N. Reinecke, E. Clark, M.K. Sunkara, T.F. Jaramillo, Core–shell $MoO_3$ –$MoS_2$ nanowires for hydrogen evolution: a functional design for electrocatalytic materials, Nano Lett. 11 (2011) 4168–4175, https://doi.org/10.1021/nl2020476.
[46] D. Voiry, M. Salehi, R. Silva, T. Fujita, M. Chen, T. Asefa, V.B. Shenoy, G. Eda, M. Chhowalla, Conducting $MoS_2$ nanosheets as catalysts for hydrogen evolution reaction, Nano Lett. 13 (2013) 6222–6227, https://doi.org/10.1021/nl403661s.
[47] E.B. Castro, M.J. De Giz, E.R. Gonzalez, J.R. Vilche, An electrochemical impedance study on the kinetics and mechanism of the hydrogen evolution reaction on nickel molybdenite electrodes, Electrochim. Acta 42 (1997) 951–959, https://doi.org/10.1016/S0013-4686(96)00272-1.
[48] G.J. Brug, A.L.G. van den Eeden, M. Sluyters-Rehbach, J.H. Sluyters, The analysis of electrode impedances complicated by the presence of a constant phase element, J. Electroanal. Chem. 176 (1984) 275–295, https://doi.org/10.1016/S0022-0728(84)80324-1.
[49] J.D. Benck, Z. Chen, L.Y. Kuritzky, A.J. Forman, T.F. Jaramillo, Amorphous molybdenum sulfide catalysts for electrochemical hydrogen production: insights into the origin of their catalytic activity, ACS Catal. 2 (2012) 1916–1923, https://doi.org/10.1021/cs300451q.
[50] B.E. Conway, B.V. Tilak, Interfacial processes involving electrocatalytic evolution and oxidation of H2, and the role of chemisorbed H, Electrochim, Acta 47 (2002) 3571–3594, https://doi.org/10.1016/S0013-4686(02)00329-8.
[51] L. Liao, J. Zhu, X. Bian, L. Zhu, M.D. Scanlon, H.H. Girault, B. Liu, MoS2 formed on mesoporous graphene as a highly active catalyst for hydrogen evolution, Adv. Funct. Mater. 23 (2013) 5326–5333, https://doi.org/10.1002/adfm.201300318.